Nature Structural & Molecular Biology doi:10.1038/nsmb.2037

Min protein patterns emerge from rapid rebinding and membrane interaction of MinE

Supplementary Information

Martin Loose,[1,2] Elisabeth Fischer-Friedrich,[3] Christoph Herold,[1]
Karsten Kruse[4], Petra Schwille [1,2*]

April 13, 2011

[1]Biophysics, BIOTEC, Dresden University of Technology, Tatzberg 47-51, 01307 Dresden, Germany

[2]Max-Planck-Institute for Molecular Cell Biology and Genetics, Pfotenhauer Str. 108, 01307 Dresden, Germany

[3]Weizmann Institute of Science, Department of Physical Chemistry, Perlman Building, Office 519b, Rehovot 76100, Israel

[4]Theoretische Physik, Universität des Saarlandes, Postfach 151150, 66041 Saarbrücken, Germany

[*]To whom correspondence should be addressed: E-mail: petra.schwille@biotec.tu-dresden.de (P.S.)

Supplementary Figures

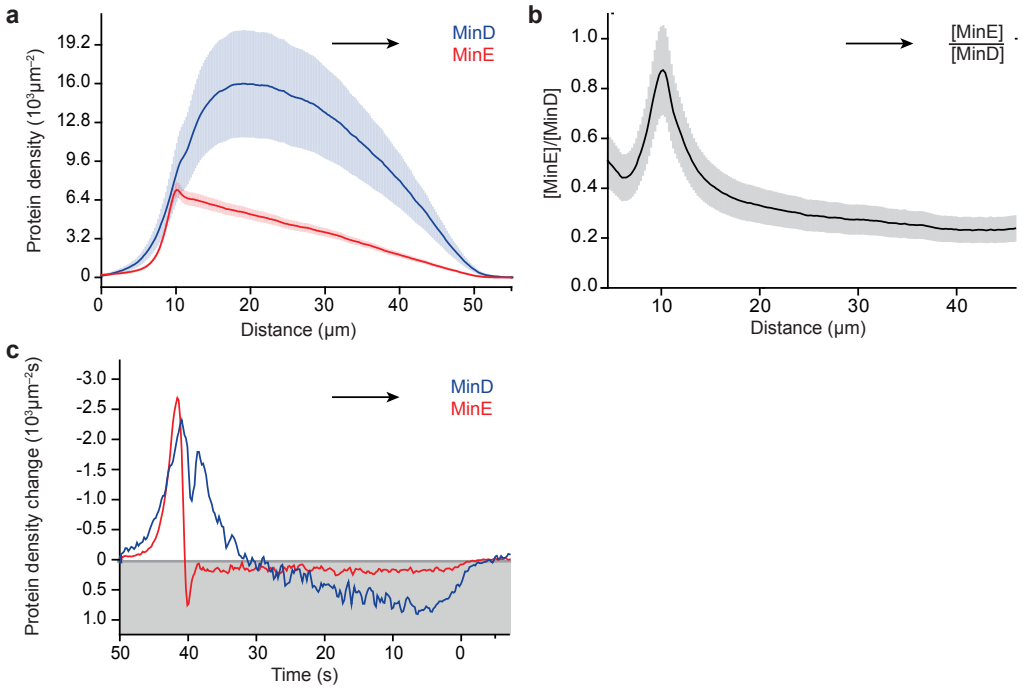

Figure 1: Quantification of protein surface densities. **(a)** Estimated surface densities of MinD (blue line) and MinE (red line) during wave propagation. Errors represent s.e.m., with n=4. **(b)** Ratio of the MinE and MinD surface densities ([MinE]/[MinD]) in the traveling protein band. The ratio continuously rises and peaks at the rear of the wave at a value of 0.87 ± 0.174. **(c)** The derivative of the estimated protein densities illustrates the density changes of MinE and MinD during wave propagation. Black arrows show the traveling direction.

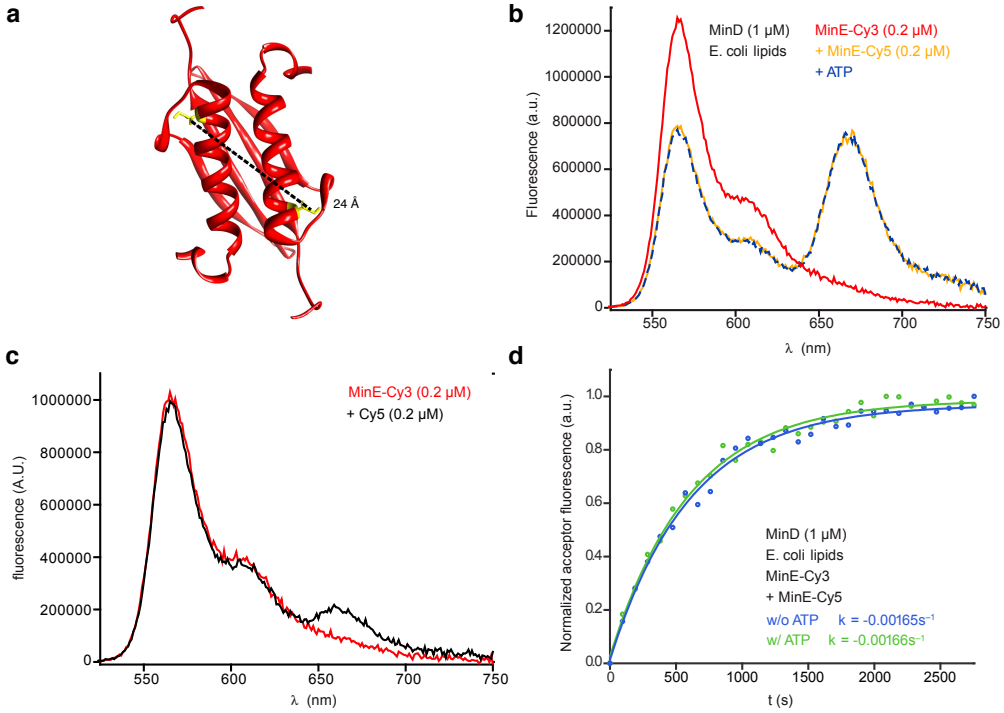

Figure 2: Spectrophotometric FRET experiments showing that the MinE monomer-dimer equilibrium is not influenced by binding to MinD. **(a)** Structure of the Topological Specificity Domain (TSD) of MinE[1]. Both Cys51 used for labeling are coloured yellow. The distance between them is about 2.4 nm. **(b)** Fluorescence spectra of MinE-Cy3 (donor) in the presence of MinD and *E. coli* lipids, before (red) and after addition (orange) of MinE-Cy5 (acceptor). While the donor fluorescence decreases after addition of MinE labeled with the donor fluorophor, the addition of ATP, which leads to MinDE complex formation on the membrane, did not change the spectrum (dashed blue line). **(c)** Control measurement of MinE-Cy3 (donor) before and after addition of the dye Cy5. The donor fluorescence is not decreased, the small peak at 665 nm corresponds to cross-excitation of Cy5. **(d)** Increase in acceptor fluorescence over time. t=0 corresponds to the first spectrum taken after addition of the acceptor. In the presence of ATP, MinD binds to the membrane and MinE binds to membrane bound MinD. This did not change the rate of equilibration.

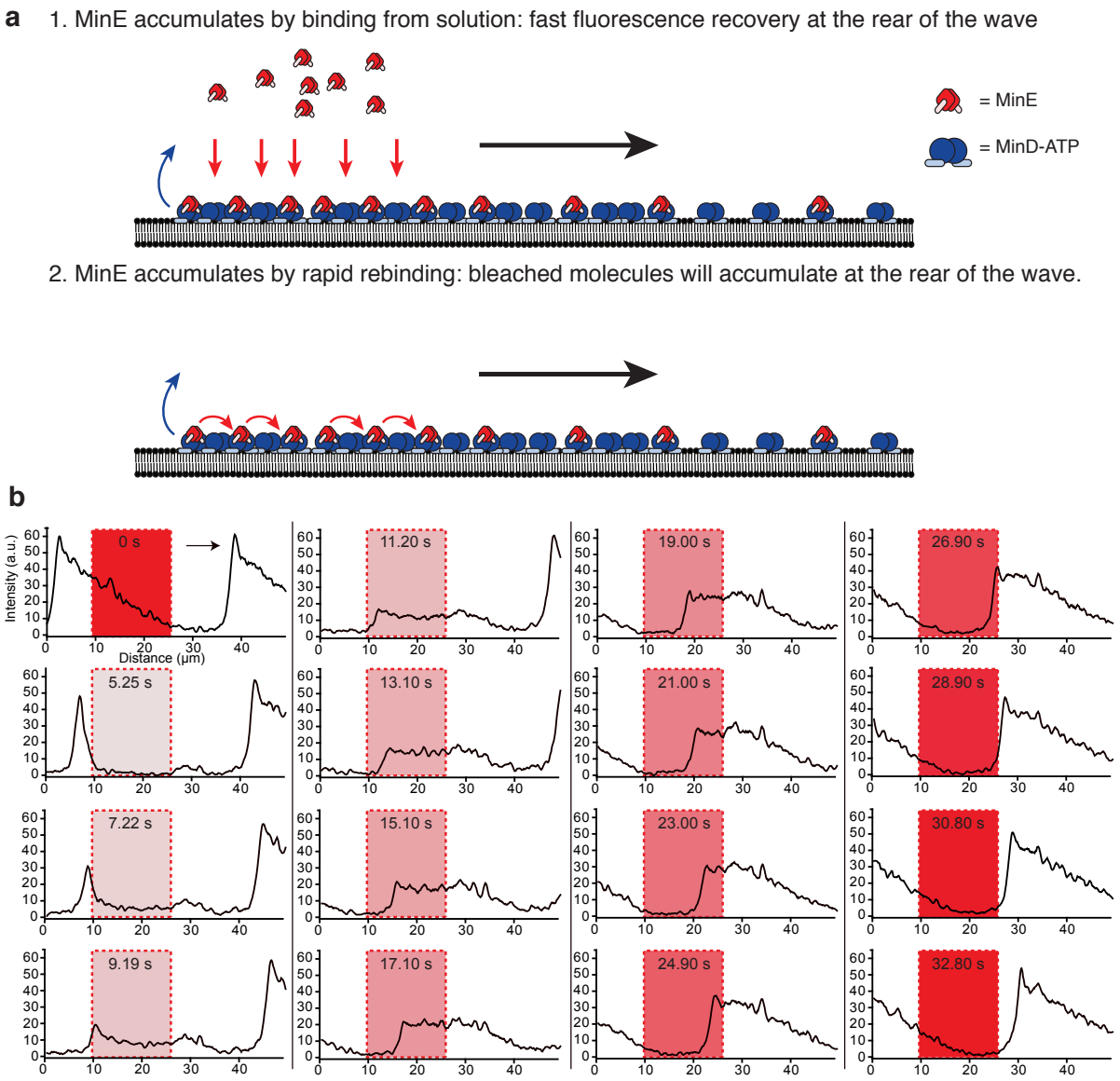

Figure 3: Photobleaching of MinE illustrates the contribution of rapid rebinding and binding of MinE from bulk solution to MinE accumulation. (a) *Top*: If MinE rebinding to MinD was negligible, MinE would completely detach from the membrane after the stimulation of MinD and diffuse away. This loss of MinE must be overcompensated by MinE present in solution, since the density of MinE increases towards the rear of the wave. Therefore we would expect a fast recovery of fluorescence after photobleaching. *Bottom*: If rebinding of MinE occurs fast on the time scale of wave propagation, bleached MinE molecules will remain incorporated in the traveling protein band and eventually accumulate at its rear. Fluorescence recovery would therefore be relatively slow. Black arrows indicate the traveling direction of the wave. **(b)** Photobleaching experiment: MinE located in the middle of the wave was bleached. While the wave was progressing, the fluorescence intensity dropped in its rear, consistent with the idea of MinE molecules remaining within the protein band by rapid rebinding. Only after the wave had left the previously bleached area, the intensity was fully recovered.

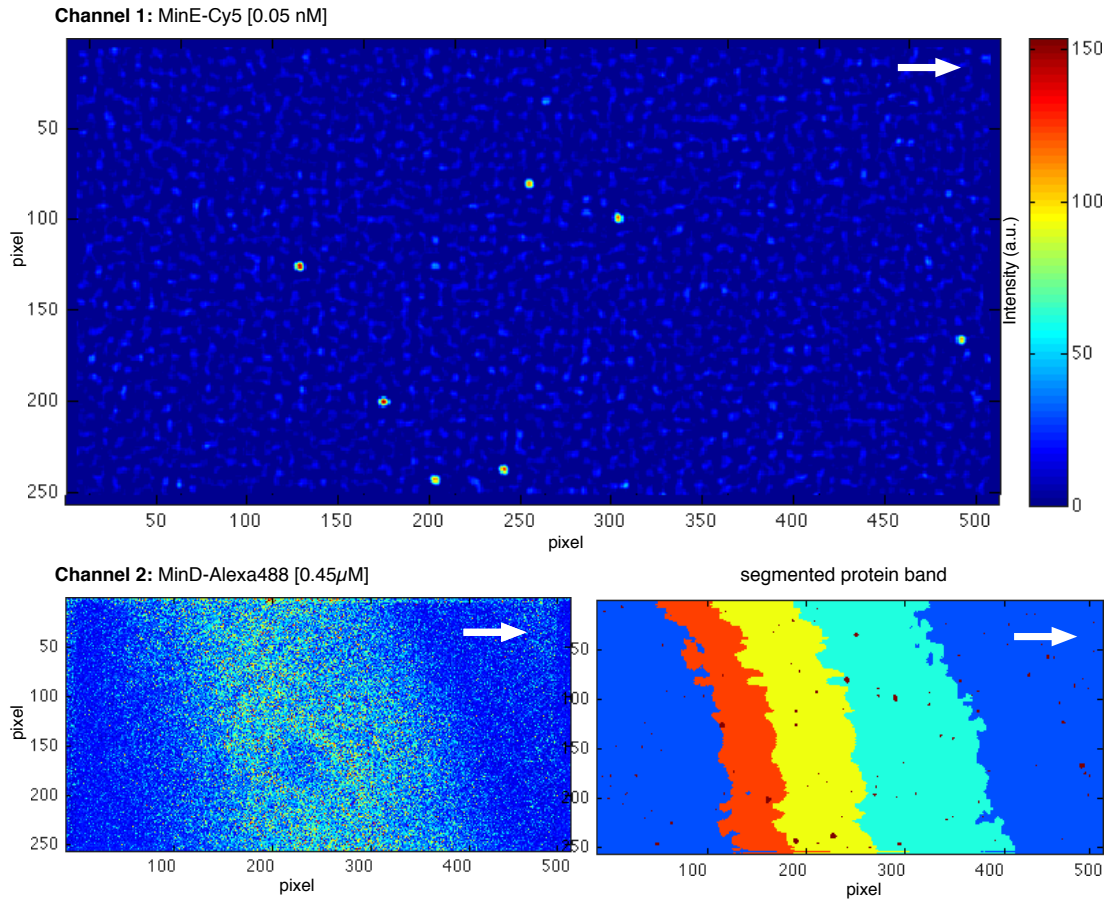

Figure 4: Screenshot of the Matlab software used to track and analyze dynamics of single Min proteins during wave propagation. Channel 1 shows single molecules, while Channel 2 the homogenous intensity of the wave, which is segmented into three different parts: 20% of the rear, 30% of the middle and 50% of the front of the wave (right). White arrows indicates the direction of the traveling wave.

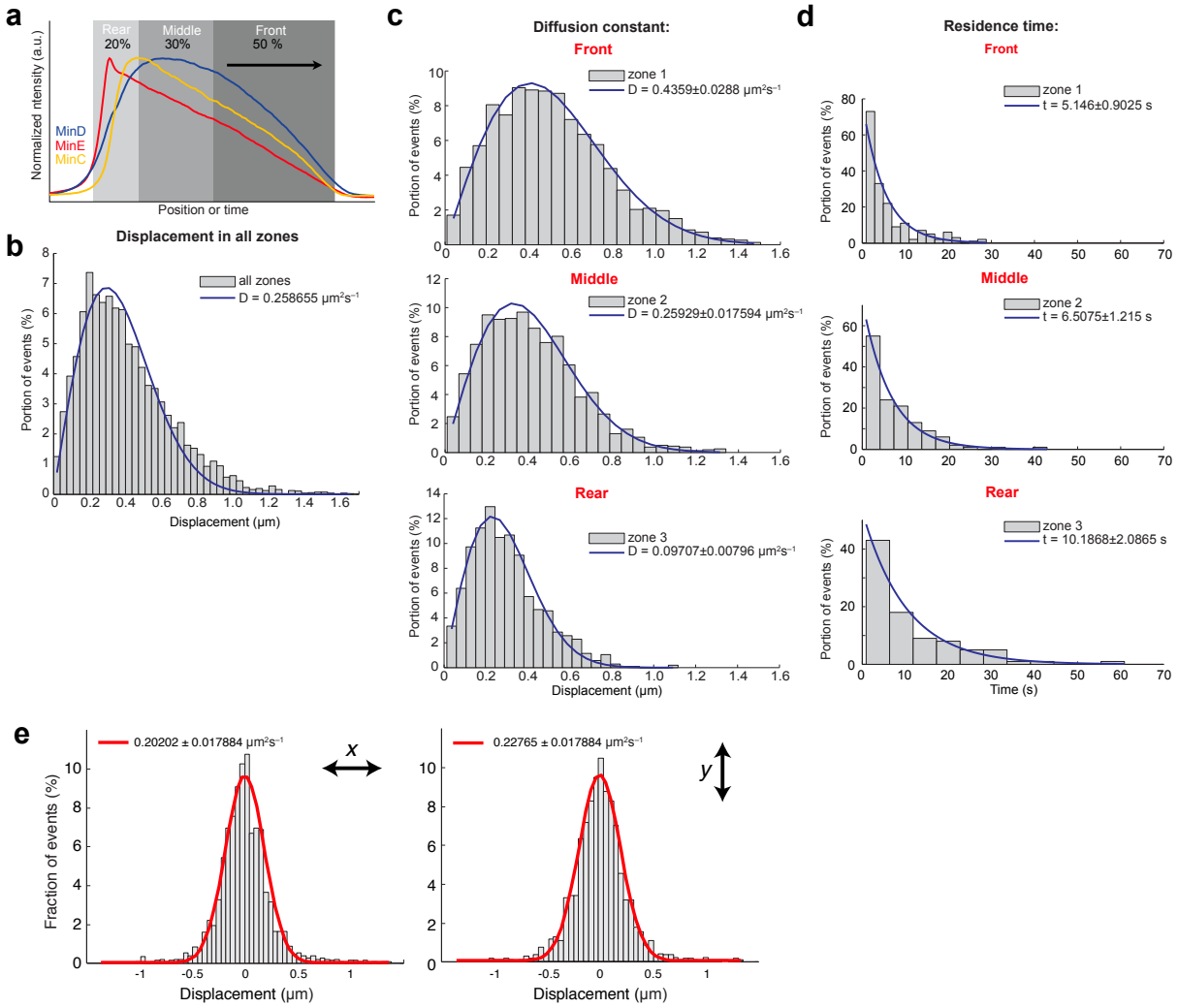

Figure 5: Results of single molecule tracking of single Min proteins during wave propagation. **(a)** Normalized intensity profiles of the waves corresponding to the profiles shown in Fig. 2 of the main text. Different shades of grey in the background indicate the different segments of the waves. **(b)** Example for a histogram of the displacements of MinE proteins found in all parts of the waves and fitted to a Rayleigh distribution. Marked deviations from the Rayleigh fit can be seen for large (>0.7 μm) and small (<0.3 μm) displacements. **(c)** Histograms of displacement of MinE proteins found in the three parts indicated in **(a)**. Towards the end of the wave, the mobility of the proteins decreases. **(e)** Histograms of x- and y- displacements of MinD-Cy5 found in the rear of a protein wave indicating isotropic diffusion of membrane-bound proteins. $\Delta t = 0.2s$ in all cases.

	part of wave	diffusion constant [$\mu m^2 s^{-1}$]	residence time [s]
MinD	rear	0.374 ± 0.022	9.02 ± 0.59
(n = 10)	middle	0.285 ± 0.021	6.87 ± 0.44
	front	0.180 ± 0.016	4.84 ± 0.31
MinE	rear	0.320 ± 0.023	12.36 ± 1.05
(n = 10)	middle	0.224 ± 0.016	8.68 ± 0.84
	front	0.143 ± 0.013	6.32 ± 0.78
MinC	rear	0.285 ± 0.012	4.66 ± 0.26
(n = 7)	middle	0.231 ± 0.012	4.56 ± 0.27
	front	0.144 ± 0.017	4.63 ± 0.29

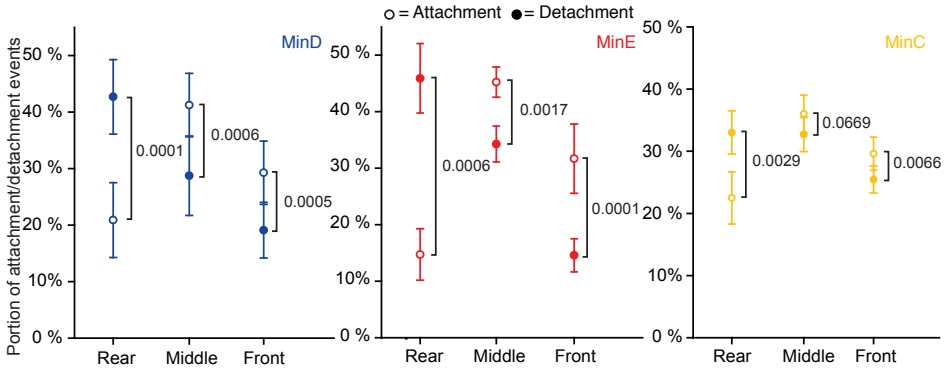

Figure 6: Results of single molecule tracking of single Min proteins during wave propagation. *Top*: Diffusion constants and residence times of Min proteins in different parts of the traveling waves determined by single molecule experiments. *Bottom*: Portion of attachment and detachment events in different segments of the traveling protein band and statistical testing of the values. Errors correspond to s.e.m., numbers show p values calculated with an unpaired t test.

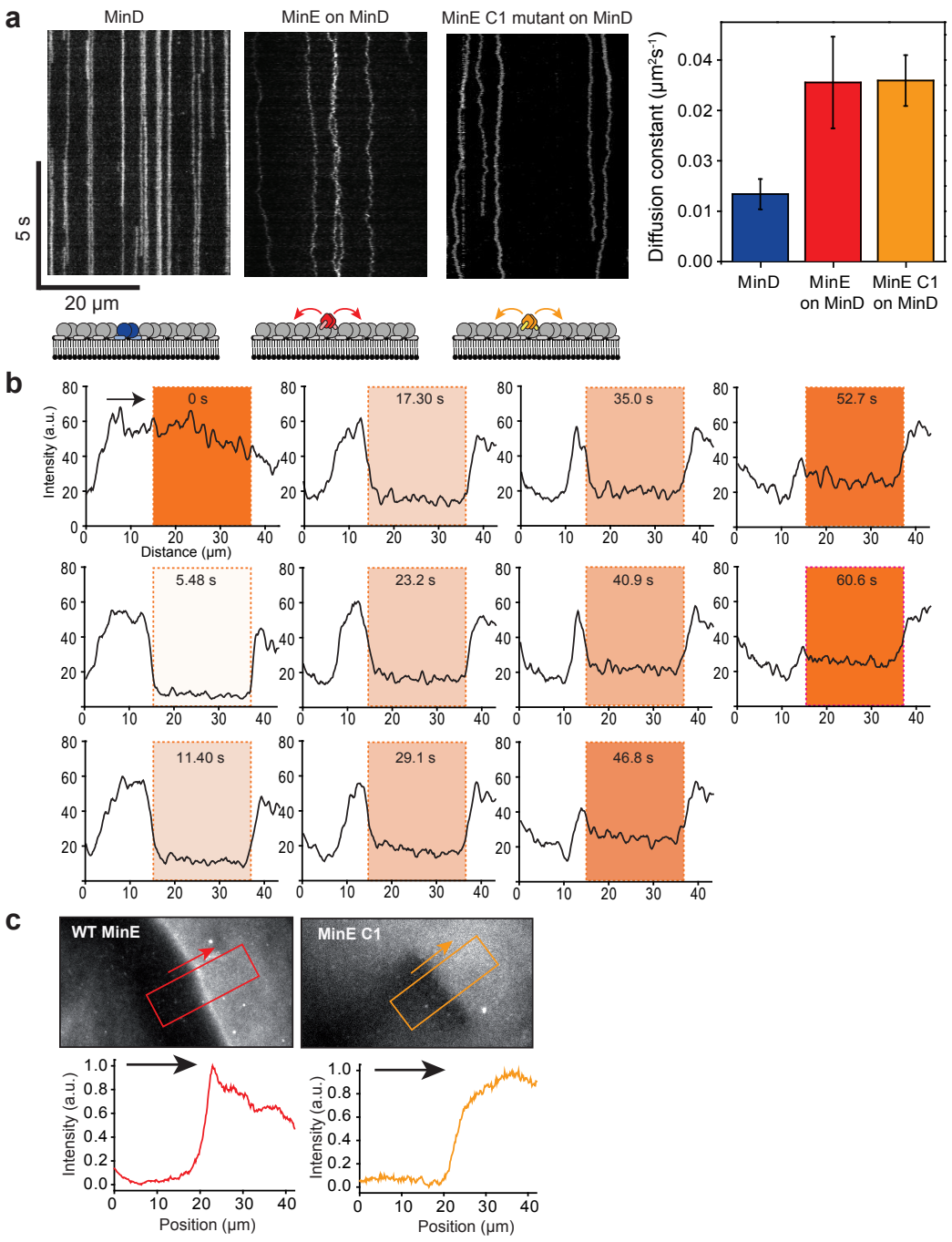

Figure 7: Comparison between MinE and MinE C1 mutant. **(a)** In the absence of waves, MinE and the membrane-binding deficient mutant MinE C1 (R10G, K10E, K10E) are able to diffuse on a saturated MinD carpet, where MinD itself does not diffuse. Kymographs show diffusion of single molecules, after adding 0.2 nM of Cy5-labeled protein to a membrane incubated with 1.3 μM MinD in the presence of ATP. Corresponding diffusion constants are illustrated in column chart. Error corresponds to s.e.m., n = 4. **(b)** FRAP experiment corresponding to Fig. 3, but in pattern formed by MinD and the MinE C1 mutant. Similar to wildtype MinE, the intensity of MinE C1 located at the rear of the wave drops after molecules in the middle were bleached, indicating that persistent binding of MinE does not require membrane binding of MinE. **(c)**TIRF micrographs of WT MinE and the MinE C1 mutant during pattern formation (left) and corresponding intensity profile plots (right). In contrast to WT MinE, no regular surface waves were formed and the density of MinE C1 did not show a peak at the rear of the wave.

Supplementary Movie captions

Movie 1: Confocal fluorescence micrographs showing waves of MinD (0.8 μM with 10 mol % MinD-Cy3), MinE (1.2 μM MinE with 10 mol % MinE-Cy5) and eGFP-MinC (0.02 μM) on a supported lipid membrane. Scale bar is 50 μm.

Movie 2: TIRF micrograph of waves of MinD (0.8 μM, doped with 5 mol % MinD-Alexa 488) and MinE (1.2 μM MinE, doped with 5 mol % MinE-Cy5) middle. The merged channels are shown on the bottom. Scale bar is 10 μm.

Movie 3: Single molecule TIRF micrograph of waves of MinE (1.2 μM, doped with 0.01 mol % MinE-Cy5) (top) and MinD (0.8 μM, doped with 10 mol % MinD-Alexa 488) (middle) and overlay (bottom). Scale bar is 20 μm.

Movie 4: Matlab based particle tracking allowed us to track and analyze single particles inside the waves. The movie shows the calculated trajectories for single MinE proteins.

Movie 5: Confocal fluorescence micrographs showing waves of MinD (blue, 0.8 μM with 10 mol % MinD-Alexa 488), MinE C1 (red, 1.2 μM MinE C1 with 10 mol % MinE C1-Cy5). Scale bar is 50 μm.

Supplementary Methods

Estimation of protein surface densities

Protein densities were estimated according to Galush *et al.*[2]. In brief, the fluorescence intensities of membrane-bound Alexa 488-labeled proteins (MinD or MinE) within a traveling wave were compared to a series of supported bilayer standards made from DOPC (Avanti Polar Lipids, Alabaster, AL) containing different amounts of Bodipy-labeled DHPE (Invitrogen). To avoid variability due to different thicknesses of mica, the membranes used for the bilayer standards and Min protein self-organization were not prepared on mica surfaces, but on cleaned and air plasma treated glass cover slips. The fluorescent membranes and protein waves were then imaged by TIRF microscopy, such that only the fluorescence of membrane-bound proteins was captured.

Following this protocol, we found that the MinD peak intensity level corresponds to a coverage density approximately $1.62 \times 10^4 \mu m^{-2} \pm 27.2\%$ (s.e.m., N=4) corresponding to an area of 60 nm^{-2} per individual protein. The peak surface density of MinE was about two times (2.21 $\pm 28.2\%$) less than the peak surface density of MinD: $0.73 \times 10^4 \mu m^{-2} \pm 7.6\%$. Using these values, we could rescale the intensity profiles of Fig. 2c of the main text (see Fig. 1 a), showing that at the peak of the [MinE]/[MinD] ratio the stoichiometry of MinE to MinD is about 1:1 (see Fig. 1 b).

FRET imaging by acceptor photobleaching

Photobleaching experiments were performed with an oxygen scavenger system (glucose oxidase (165 U/ml), catalase (2,170 U/ml), β-D-glucose (0.4% w/v) and Trolox (2 mM) (all purchased from Sigma) added to the buffer. For FRET experiments, we labeled Cys51 of MinE with either Cy3 or Cy5 according to the protocol of the manufacturer (GE Healthcare). Labeling ratio was between 80 mol % to 90 mol %. The acceptor (Cy5) was bleached and after subtraction of the background fluorescence and correction for the propagation of the wave, fluorescence intensities were quantified using ImageJ (Rasband, W.S., ImageJ, U. S. National Institutes of Health, Bethesda, Maryland, USA, http://rsb.info.nih.gov/ij/, 1997-

2007). FRET energy transfer efficiency (E) was calculated using the following equation:

$$E = \frac{I^{D,pb} - I^{D}}{I^{D,pb}}, \tag{1}$$

where $I^{D,pb}$ and I^{D} are the fluorescence intensities of the donor after and before bleaching, respectively[3].

Fluorometric FRET measurements

To investigate the dimerization equilibrium of MinE, we used the protein labeled with either Cy3 or Cy5. Concentrations and percentage of labeling were confirmed by Biorad assays and absorption at 552 and 665 nm. FRET measurements of dimerization were made using a spectrofluorometer from HORIBA Jobin Yvon (Kyoto, Japan) at an excitation wavelength of 515 nm. Kinetic assays were conducted by adding Cy5-labeled MinE to Cy3-labeled MinE. The zero value of the FRET signal was taken as the fluorescence 20 sec after the addition of MinE-Cy5.

Single molecule experiments

Determination of diffusion constants

In a homogeneous, two-dimensional system the diffusion of a Brownian particle characterized by a diffusion constant D is described by the distribution of distances, r, between two observations separated by the time lag, t:

$$f(r_0, r)dr = \frac{2r}{r_0(t)^2} \exp\left(-\frac{r^2}{r_0(t)^2}\right) dr, \tag{2}$$

with $r_0(t)^2 = 4D(t - \frac{t_{ex}}{3}) + 4\epsilon^2$. t_{ex} the exposure time and ϵ corresponds to a static error of position determination, which was determined according to Savin *et al.*[4].

To obtain the diffusion constants of the proteins, we plotted a histogram of displacements of particles between two successive frames. We assumed that the motion in each spatial dimension is normally distributed, uncorrelated and shows equal variance (see Fig. 5 e). In this case, the histograms can be plotted to a Rayleigh probability density function (eq. 2)[5, 6].

Determination of residence times

Residence times of the proteins on the membrane can be determined by plotting a histogram of the track lengths (i.e. in how many frames the particle can be found) and fitting a single exponential to it. The proteins were assigned to the different segments of the wave depending on where they detached from the membrane. Particles that left the observation area due to two-dimensional diffusion were not considered in our analysis. As confirmed using simulated movies of diffusing particles, crossing of particle trajectories did not bias the residence towards longer or shorter residence times. However, we found that finite observation time results in shorter observed residence times. We corrected for this systemic error using the equation: $\tau = (t_{obs} - 2\tau_{corr} + \exp(-t_{obs}/\tau_{corr}) \cdot (t_{obs} + 2\tau_{corr})) \cdot \tau_{corr}/t_{obs}$, with t_{obs} being the observation time, τ the measured residence time and τ_{corr} the corrected residence time. The proteins were assigned to the different segments of the wave depending on where they detached from the membrane At the imaging conditions we used, we found that for both fluorophores (Cy5 or eGFP) the number of fluorescent molecules within the traveling wave did not decrease as a function of observation time, suggesting that the bleaching time was longer than the time the proteins interacted with the membrane. As a further control, we decreased the frame rate during data acquisition, such that the time between two successive frames increased from 0.2 to 0.3 s. Therefore, while being bound to membrane, a fluorescently labeled protein will be less frequently excited by the laser beam. If the observed residence time was influenced by bleaching, we would observe longer residence times at a lower frame rate. However, we did not see a significant difference in the values obtained for either MinD, MinE or eGFP-MinC. In summary, this data shows that bleaching occurred on a longer time scale than the binding/unbinding events, indicating that it did not contribute significantly to the residence time measured.

Sedimentation assay

MinD (6 μM) and MinC (2 μM) were added to a suspension containing 0.5 mg/ml small unilamellar vesicles made of *E. coli* polar lipids (Avanti) and ATP in reaction buffer at room temperature. After incubation for 5 min, MinE (10 μM) was added. After an additional 10 min, vesicles were sedimented by centrifugation at 16,000 g at 20°for 10 min. The supernatant of each mixture was collected, and

the pellet was resuspended in SDS loading buffer to the original volume. Samples were analyzed after sodium dodecyl sulfate-polyacrylamide gel electrophoresis (SDS-PAGE) and Coomassie staining.

Supplementary Discussion

MinE FRET experiments

As shown in the main text, the fluorescence increase of the donor after bleaching of the acceptor indicates that MinE binds to MinD as a dimer. To determine if MinE exists as a monomer in solution and dimerizes upon binding to MinD, we added a population of MinE labeled with Cy3 (0.165 μM, with 77 mol % labeled MinE), a FRET donor, to a mixture of MinD and phospholipids. Then, we added an equal amount of MinE labeled with Cy5, a FRET acceptor (0.126 μM, with 83 mol % labeled MinE). If MinE preferentially exists as a dimer, the acceptor fluorescence (at 665 nm) should increase and the donor fluorescence (at 563 nm) should decrease after mixing of these two populations. Indeed, after about 40 min incubation time, the system had reached equilibrium and a decrease in donor fluorescence of 37.23 % $\pm$ 7.9 % (s.d., N = 6) was observed. Since the fraction of labeled acceptor in these experiments was 40 mol %, this FRET efficiency suggests that all MinE molecules are present in dimers. Then, we added ATP to the system, where upon MinD binds to the membrane and recruits MinE. If the monomer-dimer equilibrium of MinE was influenced by its binding to MinD, we should see a change in the donor and acceptor intensities. This means in the case of MinE monomers binding to MinD a decrease in acceptor fluorescence and an increase in donor fluorescence. However, the fluorescence intensities at 563 nm and 665 nm did not change, suggesting that the equilibrium was not influenced by MinE binding to MinD. As a control, we performed the same experiment, but instead of adding MinE-Cy5 to the system we added Cy5 alone, not being attached to MinE. In this case, no FRET occured (Fig. 2c).

Next, we tested if the rate of the equilibration changes due to binding of MinE to membrane-bound MinD. If the binding of MinE to MinD on the membrane complexes results in the formation of MinE monomers, which again dimerize following release from the membrane, MinD would act as a catalyst for MinE monomer exchange. This would increase the rate of equilibration, but the FRET efficiency at equilibrium would be the same.

To a population of MinE-Cy3 in a mixture with MinD and phospholipids, we added MinE-Cy5 and followed the increase in acceptor fluorescence (with t=0 corresponding to the first spectrum taken after

addition of the acceptor). Then, we fitted the resulting graph to an equation for a first order increase:

$$f = a(1 - e^{-kx}) \tag{3}$$

We could not observe a significant difference in the rate k depending on the presence or absence of ATP (-1.35$\times 10^{-3} \pm$ 0.42$\times 10^{-3}$ s^{-1} and -1.5$\times 10^{-3} \pm$ 0.23$\times 10^{-3}$ s^{-1} (s.d., N=3), respectively), as shown in Fig. 2d, indicating that the MinE monomer-dimer equilibrium is not influenced by binding to MinD and that only the MinE dimer has a functional role during Min oscillations.

In conclusion, our FRET experiments showed that the accumulation of MinE does not occur due to dimerization of MinE, since MinE always binds as a dimer to MinD.

Rapid rebinding of MinE versus MinE binding from solution

According to the idea of persistent binding of MinE to explain MinE accumulation, MinE already recruited to the membrane can substantially contribute binding of MinE present in solution. We performed two complementary experiments to investigate the collective dynamics of MinE during wave propagation:

First, by adding fluorescently labeled MinE to already existing protein patterns, we could directly visualize where MinE coming form solution is preferentially incorporated into the traveling wave. As described in the main text (Fig. 3), the fluorescence initially increased in the front of the wave, suggesting that bulk MinE can compete with MinE bound to the protein band only in this part of the wave, where the [MinE]/[MinD] ratio is low.

Next, we performed a photobleaching experiment, to test how fast MinE present in the wave is exchanged with MinE from bulk solution. If MinE can persistently bind to the MinD carpet, fluorescence recovery should be slow, since bleached MinE molecules will remain incorporated in the traveling protein band. Since the wave continues traveling, the bleached molecules should accumulate at the rear of the wave due to persistent binding. In contrast, if MinE does not bind persistently, but is rapidly exchanged with MinE present in bulk, it should detach and be quickly replaced by non-bleached MinE present in solution.

Consistent with the idea of persistent binding, we found that the molecules bleached in the middle of the wave remain within the protein band while the wave is progressing forward. Remarkably, we observed

the MinE peak to disappear if the rear of the MinE wave moves into the previously bleached area (Fig. 3 b, t = 11.2 s, x $\approx$ 12μm), meaning that it is mainly constituted of bleached MinE proteins. Only after the wave has left the previously bleached area, the fluorescence intensity fully recovered (Fig. 3 b). We observed the same result for the membrane-binding mutant of MinE, MinE C1 (Fig. 7).

These two results strongly support the idea of MinE persistently binding to the MinD carpet. Furthermore, this results shows that direct membrane binding of MinE is not required for persistent binding of MinE.

Bibliography

1. G. F. King, *et al.*, *Nat Struct Biol* **7**, 1013 (2000).

2. W. J. Galush, J. A. Nye, J. T. Groves, *Biophys J* **95**, 2512 (2008).

3. P. J. Verveer, O. Rocks, A. G. Harpur, P. I. Bastiaens, *Protein-Protein Interactions: A Molecular Cloning Manual*, E. Golemis, P. D. Adams, eds. (Cold Spring Harbor Press, Cold Spring Harbor, NY, USA, 2005), vol. 2, chap. 32, pp. 4598–4601.

4. T. Savin, P. S. Doyle, *Biophys J* **88**, 623 (2005).

5. A. Sonnleitner, G. Schutz, T. Schmidt, *Biophys J* **77**, 2638 (1999).

6. P. F. F. Almeida, W. L. C. Vaz, *Handbook of Biological Physics*, R. Lipowsky, E. Sackmann, eds. (Elsevier Science B.V., Amsterdam, NL, 1995), vol. 1, chap. 6, p. 305 ff.

7. M. Loose, E. Fischer-Friedrich, J. Ries, K. Kruse, P. Schwille, *Science* **320**, 789 (2008).